Article

# Solubility of Carbon Dioxide, Hydrogen Sulfide, Methane, and Nitrogen in Monoethylene Glycol; Experiments and Molecular Simulation

Noura Dawass, Ricardo R. Wanderley, Mahinder Ramdin, Othonas A. Moultos, Hanna K. Knuutila, and Thijs J. H. Vlugt*

Cite This: https://dx.doi.org/10.1021/acs.jced.0c00771

Read Online

ACCESS | Metrics & More | Article Recommendations | Supporting Information

**ABSTRACT:** Knowledge on the solubility of gases, especially carbon dioxide ($CO_2$), in monoethylene glycol (MEG) is relevant for a number of industrial applications such as separation processes and gas hydrate prevention. In this study, the solubility of $CO_2$ in MEG was measured experimentally at temperatures of 333.15, 353.15, and 373.15 K. Experimental data were used to validate Monte Carlo (MC) simulations. Continuous fractional component MC simulations in the osmotic ensemble were performed to compute the solubility of $CO_2$ in MEG at the same temperatures and at pressures up to 10 bar. MC simulations were also used to study the solubility of methane ($CH_4$), hydrogen sulfide ($H_2S$), and nitrogen ($N_2$) in MEG at 373.15 K. Solubilities from experiments and simulations are in good agreement at low pressures, but deviations were observed at high pressures. Henry coefficients were also computed using MC simulations and compared to experimental values. The order of solubilities of the gases in MEG at 373.15 K was computed as $H_2S > CO_2 > CH_4 > N_2$. Force field modifications may be required to improve the prediction of solubilities of gases in MEG at high pressures and low temperatures.
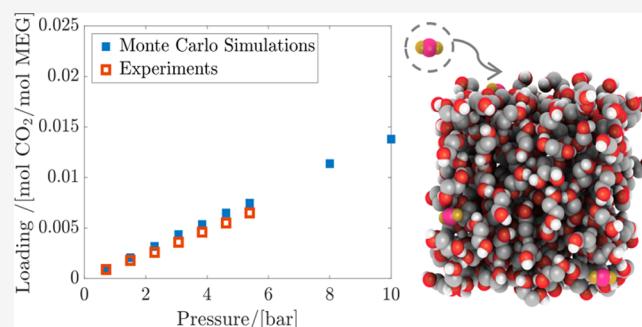
## 1. INTRODUCTION

Monoethylene glycol (MEG) is a colorless, low-volatility, and stable liquid. MEG is fully miscible in water as well as in many organic liquids such as acetone and methanol.[1] In 2020, the global market size of MEG is valued at USD 20 billion.[2] MEG is widely used as an antifreeze agent, coolant, and heat-transfer agent and as a raw material for the manufacturing of polyester fibers.[3] In the oil-and-gas industry, MEG is widely used for the prevention of gas hydrate formation.[3,4] In the course of mitigating gas hydrate formation, MEG has been reported to absorb acid gases such as carbon dioxide ($CO_2$) and hydrogen sulfide ($H_2S$).[5] Because of the absorption capability, stability, and miscibility of MEG in many organic liquids, it is also considered for use in separation processes for acid gases.[5−8]

A number of MEG-based solvents, such as deep eutectic solvents, are considered for $CO_2$ capture.[8−12] More recently, mixtures made from MEG, amines, and water are investigated for simultaneously preventing hydrate formation and removing $H_2S$ in offshore oil-and-gas applications.[13] To achieve these purposes, triethylene glycol (TEG)−amine−water mixtures were previously used. Replacing TEG with the less viscous MEG is expected to improve the absorption capability of glycols−amine−water solvents because absorption rates increase with lower viscosities.[14] To design and optimize processes in which MEG acts as a hydrate formation inhibitor

or as an absorbent, knowledge of the phase equilibria of the system is essential.[7,14] To this purpose, a number of experimental measurements of binary mixtures of MEG and gases, that is, $CO_2$ and $H_2S$, have been performed.[6,7,15] For a review of experimental studies on the solubility of acid gases in MEG, the reader is referred to ref 7.

While traditionally phase equilibrium data are obtained from experimental measurements, such an approach is not always feasible, especially if high pressures and/or temperatures are required, and when dangerous gases, such as $H_2S$, are involved. For this reason, theoretical approaches for computing the phase equilibria of mixtures of gases and liquids have been widely used.[16−19] Unlike classical thermodynamic models, molecular-based methods account for the strong molecular interactions present in associating liquids.[5] In the past few decades, molecular simulation has emerged as a powerful tool for using microscopic information of associating liquids to

predict their macroscopic behavior.[20,21] In addition to providing thermodynamic and transport data, molecular simulation can also be used to investigate the microscopic structure of solvents and to understand absorption mechanisms.[22,23]

Monte Carlo (MC) simulations have been used to predict the solubility of gases in associating liquids.[22,24,25] MC has also been widely used to study the absorption of gases in solvents such as alcohols,[25−27] ionic liquids,[28,29] and deep eutectic solvents.[30] To the best of our knowledge, studies reporting MC simulations of the phase equilibria of small gas molecules and MEG are lacking. A possible reason for the absence of such studies is the fact that the simulation of dense liquids with strong intermolecular interactions, as in the case of MEG, is computationally demanding. MC simulations in open ensembles are often used to compute the solubility of solutes in liquids. In these ensembles, the solutes are added to or removed from the simulation box. For dense liquids and/or with the presence of strong interactions, such insertions can be challenging.[31,32] To enhance the efficiency of molecular transfers in MC simulations, Shi and Maginn[24,33] developed the continuous fractional component MC (CFCMC) simulation method. In this method, the system is expanded using a so-called fractional molecule with a coupling parameter $\lambda$ which is used to vary the interactions between the fractional molecule and the surrounding molecules. In solubility calculations, a fractional molecule is used to gradually add/remove molecules to/from the solvent.[34] The presence of a fractional molecule does not affect the prediction of thermodynamic properties of the system.[32,35] For an in-depth discussion on the CFCMC method, the reader is referred to the recent review by Rahbari et al.[36]

A prerequisite for successful MC simulations of pure and multicomponent mixtures is the use of force fields that can adequately represent inter- and intramolecular interactions. Thus, another challenge of simulating gases in associating liquids, such as MEG, is the availability of force fields that provide accurate predictions of the desired properties. One of the most commonly used force fields for a large number of gases and liquids is the transferable potentials for phase equilibria (TraPPE).[37,38] The TraPPE force field has been successfully used for the prediction of thermodynamic and transport properties of gases and liquids.[25,27,28,39−41,41−44] Cardona et al.[45] used TraPPE and other classical force fields to compute the thermodynamic properties of pure MEG. The authors found that the united-atom version of TraPPE (TraPPE-UA)[38] is able to accurately predict the thermodynamic properties of pure MEG, such as the density, isothermal compressibility, and heat of vaporization.

The objective of this paper is to investigate the ability of MEG to absorb various gas molecules relevant to industrial applications. To study the solubility of $CO_2$, calorimetric experiments are performed. MC simulations in the osmotic ensemble are carried out using the CFCMC method.[32,34] CFCMC calculations are compared to experimental measurements of $CO_2$ in MEG. In addition to $CO_2$, we study the absorption of other gases relevant to the oil-and-gas industry. MC simulations are used to predict the solubilities of $CH_4$, $N_2$, and $H_2S$ in MEG. The TraPPE-UA force field is used for MEG and gases studied in this work. In the case of the solubility of $H_2S$, we test the performance of a force field developed by Kristóf and Liszi,[46] which was used in a number of solubility studies.[47,48] For the solubilities of $CH_4$, $N_2$, and $H_2S$ in MEG,

the predictions of MC simulations are compared with experimental data from the literature and the performance of the force fields used is evaluated. For all systems, the Henry coefficients are computed using CFCMC simulations.

The paper is organized as follows: in Section 2, details related to the experimental setup are provided. In Section 3, the MC simulation methods used to compute the solubilities in MEG are explained. In Section 4.1, the experimental data and MC calculations of absorption isotherms of $CO_2$ in MEG are provided. MC simulation results of the solubility of $CH_4$, $N_2$, and $H_2S$ in MEG are shown in Section 4.2. In Section 5, the main findings of this work are summarized.

## 2. EXPERIMENTAL DETAILS

In this section, we describe the experimental setup used to measure the solubility of $CO_2$ in MEG. In Table 1, the CAS

**Table 1. CAS Registry Number and Mass Fraction Purity of Components Used in the Experimental Measurements**

| component | CAS | supplier | mass fraction |
|---|---|---|---|
| MEG | 107-21-1 | Sigma-Aldrich | 0.998 |
| carbon dioxide | 124-38-9 | AGA | 0.99999 |

registry number and mass fraction purity of MEG and $CO_2$ are provided. The apparatus used to measure $CO_2$ solubility in MEG consists of a CPA 122 calorimeter purchased from ChemiSens AB. This equipment is described in the previous works by Kim et al.[49,50] A schematic representation of this setup is shown in Figure 1. Here, we describe the experimental
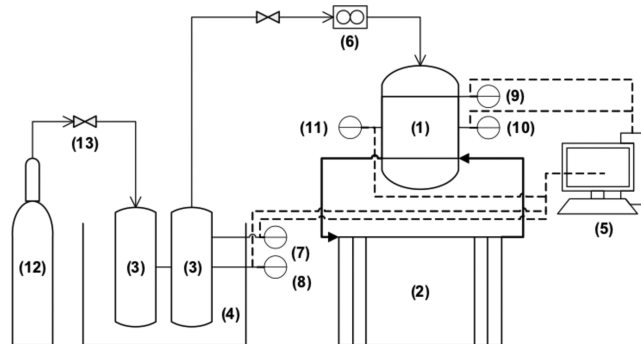


**Figure 1.** Setup of the CPA 122 calorimeter used to measure the solubility of $CO_2$ in MEG. MEG is filled in a stirred cell reactor (1) linked to a temperature controller (2). $CO_2$ is stored in two cylinders (3) that are placed in a water path (4). A computer (5) sends signals to the MFC (6) to inject $CO_2$ in the cell reactor (1). Temperature and pressure data of $CO_2$ are measured using devices 7 and 8, respectively. For MEG, devices 9 and 10 are used. The power transferred from the reactor (1) to the temperature controller is measured using device 11.

setup while referring to the number labeling (shown in the parentheses) of each device in Figure 1. Essentially, the setup consists of a large stirred cell reactor (1) of $V \approx 2$ dm$^3$ and two large cylinders (3) for storing $CO_2$ of $V \approx 4.55$ dm$^3$. The reactor is vacuumed and partially filled with ca. 1.2 dm$^3$ of the solvent at the start of each experiment. Vacuuming is performed three more times at room temperature so that only ethylene glycol vapor in equilibrium with the liquid is kept in the cell. Meanwhile, the $CO_2$ cylinders are kept in a water bath (4) coupled with a temperature controller so that their

conditions are also supervised. The temperature controller (2) is set to increase the temperature of the reactor up to a desired setpoint, and the stirrer is turned on at approximately 500 rpm. After the setpoint is reached and equilibrium is achieved for a minimum of 30 min, the first $CO_2$ injection can be performed. A computer (5) is used to send a signal to the mass flow controller (MFC) (6) allowing its opening for a short amount of time. There are temperature (7) and pressure (8) measuring devices coupled to the cylinders, and another one of each coupled to the stirred cell (9, 10). With data gathered both before and after each injection and with knowledge of the volumes of the cylinders and of the stirred cell, one is able to calculate the amount of $CO_2$ transferred to the gas phase and to the liquid phase of the reactor. For these calculations, the Peng–Robinson equation of state (PR-EOS) has been employed to correlate pressure–volume–temperature (PVT) to the number of moles ($n$). The PR-EOS requires the critical pressure $P_c$ = 73.90 bar, the critical temperature $T_c$ = 304.21 K, and the acentric factor $\omega$ = 0224, all of these values referring to pure $CO_2$. No binary interaction parameters are used for these calculations. Additionally, the volumetric flow of $CO_2$ passing through the MFC (6) is recorded by the computer (5) so that the amount of gas leaving the cylinders can be calculated either by PR-EOS or by simply reading the MFC data log. After having assessed that both methods return roughly the same values, all solubility results shown in this work have been obtained by reading the values recorded by the MFC.

The calorimeter CPA 122 is also able to record heat of absorption data from measuring (11) of the power transferred from the reactor to the temperature controller. Treatment of heat of absorption data was not performed because they are not relevant to this study. After each injection and after equilibrium is attained in the $CO_2$ cylinders, these cylinders have to be refilled with $CO_2$ from the wall (12) through opening of the valve (13). After achieving equilibrium in both cylinders and in the stirred cell, the next injection is performed and the process is repeated until the reactor approaches the maximum operational pressure of 6 bar.

The calorimeter CPA 122 does not directly deliver $CO_2$ partial pressure data but total pressure data. After each injection, it is expected that the increase in pressure measured in the reactor is solely due to an extra amount of $CO_2$ which is transferred to the gas phase and not due to any volatilization of MEG brought by the $CO_2$ injection. In other words, treatment of the solubility data requires a constant partial pressure of MEG throughout the whole experiment. There are no grounds to suspect that this assumption is unreasonable. Therefore, the partial pressure of $CO_2$ can be back-calculated by subtracting the partial pressure of MEG at the start of the experiment from the total pressure obtained after each injection.

The expanded uncertainties with a 0.95 level of confidence for the $CO_2$ solubility experiments have been evaluated as being approximately $U(\alpha)$ = 0.1, implying that $CO_2$ loadings are reported within a confidence margin of roughly 10%. A detailed procedure for the calculation of expanded uncertainties is provided in the Supporting Information of this study.

For these experiments, MEG anhydrous with a purity of 99.8% (CAS 107-21-1) has been supplied by Sigma-Aldrich and used in the procedures without further purification, while carbon dioxide of a 99.999% purity has been supplied by AGA.

## 3. MC SIMULATION DETAILS

**3.1. Force Fields.** Classical force fields were used to describe the interactions of the molecules studied in this work. For MEG, all interaction potentials and parameters follow from the TraPPE-UA force field.[38] The TraPPE force field adequately predicts densities and vapor–liquid equilibria (VLE) of many species such as normal alkanes,[37] branched alkanes,[51] glycols, and ketones.[38] To accurately represent the molecular structure of MEG, Stubbs et al.[38] added an additional repulsive term ($r^{-12}$) for interactions between a hydroxyl hydrogen and an oxygen atom separated by four bonds. In our study, the TraPPE-UA force field was used also to represent $CO_2$, $CH_4$, $H_2S$, and $N_2$ as rigid objects. We also tested another four-site model presented by Kristóf and Liszi[46] for $H_2S$, referred to here as $H_2S$-KL. The main differences between the two force fields are the nonbonded Lennard-Jones (LJ) parameters and the atomic charges. Table 2 lists the components simulated in this study and the force field used for each component. All force field parameters are listed in the Supporting Information.

**Table 2. Chemical Formulas and Force Fields of the Components Simulated in This Work**

| component | chemical formula | force field |
|---|---|---|
| MEG | $HO(CH_2)_2OH$ | TraPPE-UA[38] |
| carbon dioxide | $CO_2$ | TraPPE-UA[70] |
| methane | $CH_4$ | TraPPE-UA[37] |
| hydrogen sulfide | $H_2S$ | TraPPE-UA[69] |
| hydrogen sulfide | $H_2S$ | Kristóf and Liszi[46] |
| nitrogen | $N_2$ | TraPPE-UA[70] |

In this work, two types of intermolecular interactions are computed: LJ and Coulombic interactions. LJ interactions were truncated at 12 Å, and the uncertainty due to truncation is handled by applying analytic tail corrections.[20,21] The Lorentz–Berthelot mixing rules were used for LJ interactions between dissimilar interaction sites.[20,21] The Ewald summation method was applied to handle electrostatic interactions with a relative precision of $10^{-6}$. The real-space part of the electrostatic interactions was truncated at 12 Å. All simulations were carried out in the osmotic ensemble (see Section 3.2). The PC-SAFT equation of state was used to compute the fugacity of the solutes at the desired temperatures and pressures.[52,53]

**3.2. CFCMC Method.** The osmotic ensemble[21] is used to compute the solubility of small solute molecules in nonvolatile solvents. In this open ensemble, the following parameters are fixed: the temperature ($T$), the hydrostatic pressure ($P$), the number of molecules of MEG ($N_{MEG}$), and the fugacity of the solute ($f$). The number of molecules of the solute ($N_s$) and the volume of the system ($V$) are varied to achieve equilibrium. The hydrostatic pressure $P$ inside the simulation box corresponds to the imposed fugacity $f$ of the reservoir. An essential part of the calculations is the insertion and/or deletion of solute molecules in the simulation box. When studying dense solvents, as in the case of MEG, molecule insertions can be challenging.[31,32] To improve the probability of accepting insertion/deletion moves, the CFCMC method was used.[24,32,36,54,55] The osmotic ensemble was expanded using a so-called fractional molecule.[24] As opposed to a whole molecule, the strength of interactions of a fractional molecule is varied using a coupling parameter $\lambda$. When $\lambda$ = 0, the
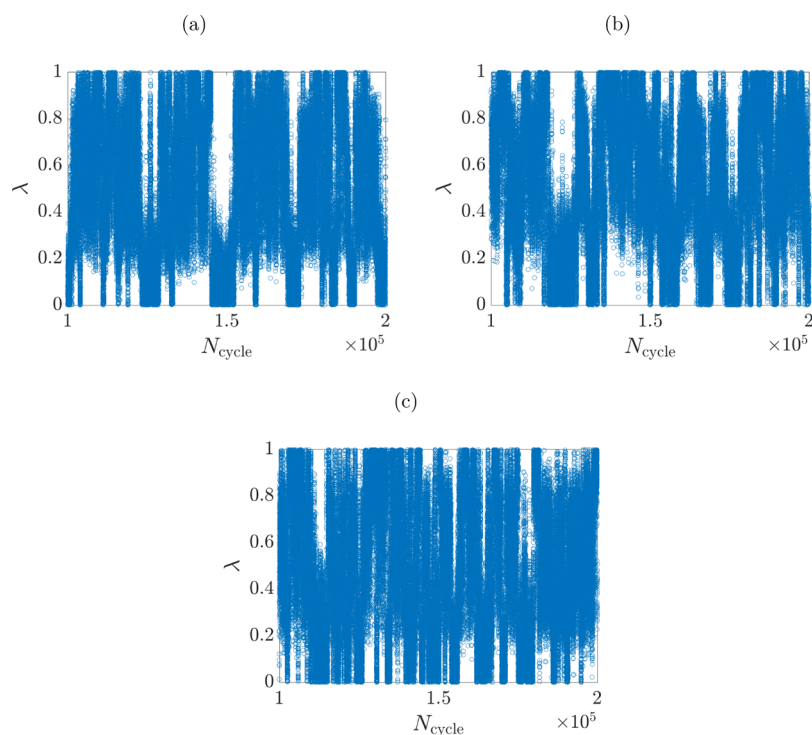
**Figure 2.** Values of $\lambda$ vs the number of MC cycles of an MEG fractional molecule in *NPT* MC simulations. To scale the interaction of the fractional molecules, the following scaling potentials are used (see eq 1): (a) 1-2-6, (b) 1-1-6, and (c) 1-1-48.

fractional molecule acts as an ideal gas molecule and does not interact with the surrounding molecules. When $\lambda = 1$, the fractional molecule fully interacts with the surrounding molecules. By varying the strength of interactions of the fractional molecule with the surrounding molecules, whole molecules can be gradually added or removed. Besides the conventional MC thermalization trial moves,[20,21] trial moves attempting to change $\lambda$ are required. Shi and Maginn[24] derived Metropolis-like acceptance rules for changing the values of $\lambda$ in the osmotic ensemble. For each solute type, a fractional molecule is used to insert/delete molecules in the simulation box. When $\lambda$ drops below 0, the fractional molecule is removed and a randomly selected whole molecule is transformed into a fractional molecule. When $\lambda$ is larger than 1, the fractional molecule is transformed into a whole molecule and a new fractional molecule is inserted.[24,33] For the solvent, a fractional molecule is used to improve sampling, while keeping the total number of molecules of the solvent fixed. For a fractional molecule of the solvent type, $\lambda$ trial moves involve changing the values of $\lambda$, random reinsertions of the fractional molecule, and identity swaps between a fractional molecule and a whole molecule.[35] In CFCMC simulations, the system is biased to ensure a flat distribution of the observed probability of $\lambda$. From the probability distribution of $\lambda$, the excess chemical potential and hence the Henry coefficient are obtained. For more details, the reader is referred to refs.[24,32,34,35]

*3.2.1. Scaling of the Intermolecular Interactions.* For each fractional molecule, a weight function $W(\lambda)$ is constructed to achieve a flat probability distribution of $\lambda$ and ensure smooth transitions between $\lambda = 0$ and $\lambda = 1$.[32] Essentially, at a certain $\lambda$, the value of $W(\lambda)$ counteracts the value of $\langle \partial U / \partial \lambda \rangle$, which is the average potential energy change with $\lambda$. Fluctuations in the value of $\partial U / \partial \lambda$ can be large, which can hinder the efficient sampling of the $\lambda$-space. As a result, a pathway that minimizes

the variance of $\partial U / \partial \lambda$ has to be chosen.[56] Changes in the values of $\lambda$ depend on how intermolecular interactions are scaled when $\lambda$ is varied[56] (intramolecular interactions are not scaled). Electrostatic interactions are scaled by using a scaling parameter $\lambda_{el}$ that is a function of $\lambda$.[34,57] For nonbonded LJ interactions, the following soft-core scaling potential is used[56,58,59]

$$u(r_{ij}, \lambda) = 4\epsilon_{ij}\lambda^a \left[ \left( \frac{1}{\alpha(1-\lambda)^b + \left(\frac{r_{ij}}{\sigma_{ij}}\right)^c} \right)^{12/c} - \left( \frac{1}{\alpha(1-\lambda)^b + \left(\frac{r_{ij}}{\sigma_{ij}}\right)^c} \right)^{6/c} \right]$$

(1)

where $i$ and $j$ are the interaction sites, $\epsilon_{ij}$ and $\sigma_{ij}$ are the LJ parameters, and $r_{ij}$ is the distance between $i$ and $j$. The parameters $a$, $b$, $c$, and $\alpha$ are adjusted to achieve an efficient sampling of the $\lambda$-space. For systems composed of MEG molecules, a number of scaling potentials were tested. Figure 2 shows the values of $\lambda$ of an MEG fractional as a function of the number of MC cycles for three scaling potentials. The commonly used 1-2-6 potential results in poor sampling of the $\lambda$-space. Figure 2a shows that at certain periods, the values of $\lambda$ are confined to a limited range. Changing the parameter $b$ from 2 to 1 improves the sampling as demonstrated in Figure 2b. Figure 2c shows that the 1-1-48 potential with $\alpha = 0.0025$, which was recommended earlier by Pham et al.,[56] results in the best sampling.

**Table 3. Properties of Pure MEG at Different Temperatures from Experiments and MC Simulations[a]**

| $T$ [K] | $\rho^L_{exp}$ [kg/m³] | $\rho^L_{sim}$ [kg/m³] | $\mu^{ex}/k_B$ [K] | $\rho^V_{sim}$ [kg/m³] | $P^{sat}_{sim}$ [bar] | $P^{sat}_{NIST}$ [bar] |
|---|---|---|---|---|---|---|
| 333.15 | 1085 | 1029.1 ± 20 | −4125 ± 41 | 4.2 × 10⁻⁶ | 0.022 | 0.021 |
| 353.15 | 1070.1 | 1016.3 ± 0.5 | −3948 ± 25 | 1.4 × 10⁻⁵ | 0.0068 | 0.0067 |
| 373.15 | | 1003.3 ± 0.5 | −3749 ± 27 | 4.3 × 10⁻⁵ | 0.0019 | 0.0018 |

[a]Density of pure MEG in kg/m³ obtained from experiments[13] and MC simulations at $P$ = 1 bar. The vapor densities and saturated vapor pressures of MEG are computed from $\mu^{ex}/[k_B T]$ (see Section 4.1). Experimental vapor pressures are obtained from the NIST database.[60]

**3.3. Simulation Details.** Molecular simulations were performed using the recently developed open-source software package Brick-CFCMC.[34] The density of pure MEG was computed in the *NPT* ensemble at 1 bar and at temperatures of 333.15 and 353.15 K. The solubility of $CO_2$ in MEG was computed at three temperatures, $T$ = 333.15, 353.15, and 373.15 K. The solubilities of $CH_4$, $N_2$, and $H_2S$ in MEG were computed at $T$ = 373.15 K. For all gases, solubilities were computed at pressures ranging from 1 to 10 bar, but in the case of $N_2$, pressures up to 100 bar were considered because $N_2$ has very low solubilities in MEG at low pressures. Simulation boxes were set up with 250−350 MEG molecules depending on the number of solute molecules absorbed. Two fractional molecules were used: a fractional molecule to insert/remove solute molecules into the simulation box and a MEG fractional molecule. Adding an MEG fractional to the simulation box has the following advantages: (1) it enhances sampling as the fractional molecule can be used for random reinsertions (low $\lambda$) and identity changes (high $\lambda$) and (2) the excess chemical potential of MEG is automatically computed, from which the saturated vapor pressure of MEG can be estimated. The following MC trial moves were used: translations, rotations, and volume change trial moves. MC trial moves that attempt to change the values of $\lambda$ were used for both fractional molecules. Simulations in the osmotic ensemble were carried out with the following probabilities for selecting trial moves: 25% translations, 25% rotations, 32% intramolecular moves, 1% volume changes, and 17% $\lambda$ trial moves (divided equally between the solute and MEG fractional molecules). A minimum of $1 \times 10^6$ cycles were carried out for equilibration. At each MC cycle, the number of the trial moves performed equals the number of molecules of the system.

During equilibration, an iterative scheme was used to obtain a weight function $W(\lambda)$ that results in a flat probability distribution of $\lambda$. For production runs, $1 \times 10^6$ cycles were carried out. To minimize the statistical error of the computed averages, a number of independent production simulations were performed at a specified $T$ and $P$. The number of simulations performed was selected such that the uncertainty is less than 5%. For each system simulated in this work, at least 25 independent production runs were carried out. Error bars were computed by dividing these runs into five groups and calculating the standard deviation.[21] For each system, these error bars are reported in the Supporting Information (Tables S14−S19).

## 4. RESULTS AND DISCUSSION

**4.1. Solubility of $CO_2$ in MEG from Experiments and MC Simulations.** Densities of pure MEG were computed using MC simulations in the *NPT* ensemble at $P$ = 1 bar and at $T$ = 333.15 K and $T$ = 353.15 K. In Table 3, densities (reported in units of kg/m³) from simulations are compared to experimental values from the work of Skylogianni et al.[13] Table 3 shows that when using the TraPPE-UA force field,

simulations underpredict the densities of MEG. The differences between experiments and simulations are around 5%. Simulating a solvent with an underestimated density may result in higher absorption capacity. Deviations between experiments and simulations will be discussed in detail later in this section.

As a fractional MEG molecule is present in the simulation, we can calculate the excess chemical potential of MEG $\mu^{ex}$ from the probability distribution of its $\lambda$ parameter. The chemical potential of MEG in the liquid phase equals[35]

$$\mu^L = \mu^o + k_B T \ln \frac{\rho^L}{\rho^o} + \mu^{ex} \tag{2}$$

where $\rho^L$ is the number density of MEG and $\mu^o$ is the ideal gas chemical potential, which only depends on the temperature.[21] Equation 2 also applies to MEG in the gas phase. At equilibrium, the chemical potentials in the liquid phase and gas phase are equal. If we assume an ideal gas phase, then $\mu^{ex}$ in the gas phase equals 0 and $\rho^V = P^{sat}/k_B T$. From this, the saturated vapor pressure $P^{sat}$ of MEG can be estimated (eq. S7 in the Supporting Information). In Table 3, we report the excess chemical potential, vapor densities, and saturated vapor pressures of pure MEG. The vapor pressures computed from MC simulations are compared to experimental values obtained from the NIST database.[60] Table 3 shows that both methods are in good agreement. The pressures reported in Table 3 can be considered very small, which validates the assumption made by the experimental method regarding the nonvolatility of MEG.

Figure 3 shows absorption isotherms of $CO_2$ in MEG from experiments and MC simulations in the osmotic ensemble at the temperatures of $T$ = 333.15 K, $T$ = 353.15 K, and $T$ = 373.15 K. In Figure 4, a typical MC simulation snapshot of
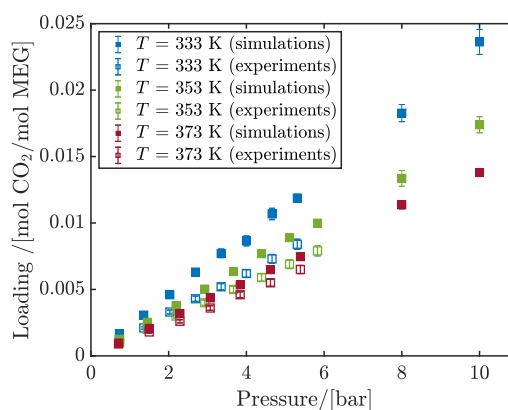


**Figure 3.** Absorption isotherms of $CO_2$ in MEG at different temperatures. Closed symbols are solubilities using MC simulations (details in Section 3), and open symbols are experimental results of this work. The raw data and the corresponding uncertainties are provided in Tables S7−S9 and S14−S16 of the Supporting Information.
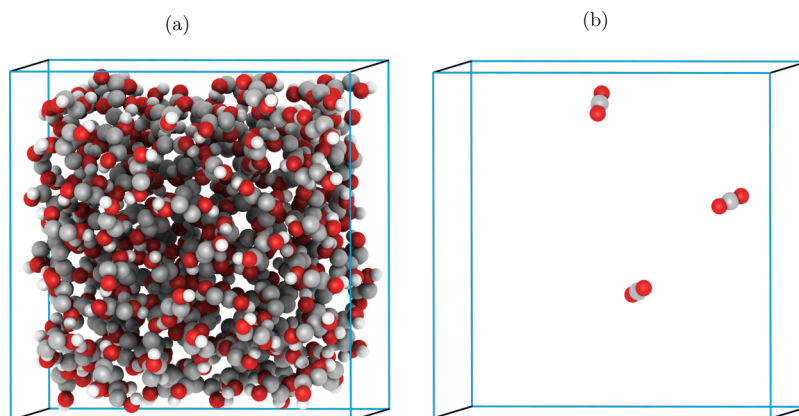
**Figure 4.** (a) Typical snapshot of a simulation of MEG in which $CO_2$ is absorbed in the osmotic ensemble ($T$ = 333 K, $P$ = 8 bar, $N_{MEG}$ = 220 molecules, and $N_{CO_2}$ = 3 molecules) in a simulation box with the dimensions of 28 × 28 × 28 Å. (b) Same snapshot as in (a) while showing only $CO_2$ molecules. Clearly, the $CO_2$ molecules are not clustered. Figures were produced using the software package iRASPA.[71]

MEG and $CO_2$ molecules is shown. Figure 4 shows that $CO_2$ molecules are dispersed in MEG and not clustered. In Figure 3, the ratio of the number of moles of $CO_2$ to the number of moles of MEG (i.e., loading) is plotted as a function of pressure. Solubilities from MC simulations were found to qualitatively agree with experimental measurements. Both experiments and simulations show that for all temperatures studied, the loading is almost linear in this pressure range. Additionally, both methods report that the absorption of $CO_2$ in MEG decreases at higher temperatures. Figure 3 shows that the quantitative agreement between MC simulations and experiments varies with temperature and pressure. At very low pressures (i.e., <2 bar), loadings of $CO_2$ obtained from MC simulations agree well with experiments. At higher pressures, MC simulations overpredict the absorption of $CO_2$ when compared to experiments. The deviation between simulations and experiments systematically increases with pressure and decreases with temperature. The inherent uncertainties of the experimental loadings of $CO_2$ in MEG are shown with vertical error bars. Uncertainties of experimental values are calculated using a methodology described in the work of Wanderley and co-workers.[61] The inherent uncertainties of the total pressure are delimited by the sensitivity of the pressure transducer employed for those measurements, which is ±0.015 bar. Conversely, this implies that the uncertainty of the estimated partial pressures of $CO_2$ is ±0.021 bar because of error propagation. One can see in Figure 3 that these are very small uncertainties when considering the span of pressures measured in the series of experiments. In the Supporting Information, solubilities from experiments and MC simulations are provided in a tabulated from along with their uncertainties.

In Figure 5, solubilities measured in this work at $T$ = 373.15 K are compared to solubilities from other experimental studies. The measurements in this work were found to match the data from Jou et al.[15] at low pressures. The experimental method of Jou et al.[15] differs from our experimental method. The main difference is that Jou et al.[15] evaluated $CO_2$ concentrations using gas chromatography and acid−base titration, while we apply a mass balance approach. At higher pressures, $CO_2$ solubilities from other experimental works slightly differ from the results of this work. Figure 5 also shows that loadings computed using MC simulations agree the most with our experimental results. In the Supporting Information (Figure
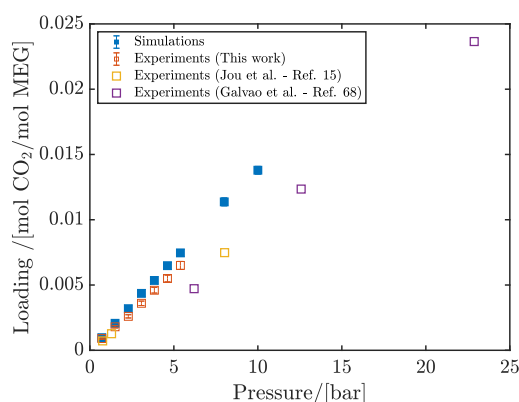


**Figure 5.** Absorption isotherm of $CO_2$ in MEG at $T$ = 373.15 K. Closed symbols are solubilities using MC simulations (details in Section 3), and open symbols are experimental results. The raw data and the corresponding uncertainties are provided in Tables S9, S10, and S16 of the Supporting Information.

S2), we compare our simulations and experimental results with other experimental data from the literature.[14,62,63]

Besides absorption isotherms, it is also possible to describe the solubility of gases in solvents through Henry coefficients. The Henry coefficient of solute 2 in solvent 1 is defined as[64]

$$H_{21} = \lim_{x_2 \to 0} \frac{P_2}{x_2} = \lim_{x_2 \to 0} \frac{f_2}{x_2} \tag{3}$$

where $P_2$ and $x_2$ are the partial pressure and mole fraction of solute 2, respectively, and $f_2$ is its fugacity. With these experimental values, the Henry coefficient is defined as the partial pressure of $CO_2$ in bar divided by the $CO_2$ molar fraction in MEG. In MC simulations, Henry coefficients $H_{21}$ are computed from the excess chemical potential of the solute $\mu_2^{ex}$[65]

$$H_{21} = \lim_{x_2 \to 0} k_B T \rho_1 \exp\left[\frac{\mu_2^{ex}}{k_B T}\right] \tag{4}$$

In CFCMC, $\mu_2^{ex}$ is computed from sampling the probability distribution of $\lambda$.[32,35] In Table 4, Henry coefficients of $CO_2$ in MEG $H_{CO_2,MEG}$ computed using MC simulations are reported at different temperatures and compared to Henry coefficients from experiments. Both methods demonstrate that the value of

**Table 4. Henry Coefficient of $CO_2$ in MEG at Different Temperatures Obtained from the Experiments (This Work) and Molecular Simulations Performed in This Work**

| $T$ [K] | $H_{CO_2,MEG}$, bar (mol $CO_2$/mol EG) | |
|---|---|---|
| | experimental | MC simulations |
| 333.15 | 634 ± 30 | 445 ± 20 |
| 353.15 | 736 ± 36 | 576 ± 15 |
| 373.15 | 843 ± 40 | 730 ± 21 |

$H_{CO_2,MEG}$ increases with temperature. The maximum difference between experimental and computed Henry coefficients is 30%. The difference consistently decreases with increasing temperature to reach 13% at $T = 373.15$ K. Predictions from MC simulations are satisfactory considering that the force fields and the mixing rules used for MEG and $CO_2$ were not modified. The Henry coefficients reported in Table 4 indicate that pure MEG would not be a good absorbent for $CO_2$. In a study by Ramdin et al.,[66] Henry coefficients at $T = 333$ K of $CO_2$ in selexol and the ionic liquid $[bmim][TF_2N]$ were reported to be 68 bar and 66 bar, respectively. At the same temperature, the experimental Henry coefficient of $CO_2$ in MEG is 634 bar (Table 4).

From the knowledge of solubility of $CO_2$ at different temperatures, the heat of absorption $q$ of $CO_2$ in MEG can be calculated using

$$\frac{-q}{R} = \frac{\partial(\ln(H_{CO_2,MEG}/P_o))}{\partial(1/T)} \tag{5}$$

where $R$ is the gas constant and $P_o$ is a reference pressure to make the argument of the logarithm dimensionless. Using solubilities of $CO_2$ in MEG from MC simulations of this work, $q$ was found to be equal to $-12.8$ kJ/mol, indicating that the absorption of $CO_2$ is an exothermic process. This value is in good agreement with experimental findings. Recently, the heat of absorption was measured using calorimetric experiments in a study by Wanderley et al.[67] and was reported to be $-14$ kJ/mol at 343.15 K.

The differences between theoretical and experimental solubilities can be attributed to the force field used to describe MEG. From our simulations, it is observed that the TraPPE-UA force field underpredicts the density of pure MEG (see Table 3). Lower MEG densities can potentially lead to higher absorption capacities of solutes. Moreover, the force field parameters of TraPPE-UA[38] were obtained using the VLE experimental data of MEG at high temperatures (>400 K), and as a result, inaccuracies at lower temperatures can be expected as we move outside the fitting range of the TraPPE force field.

Figure 3 shows that deviations between experiments and simulations are larger at lower temperatures. While deviations can be reduced by optimizing the force field parameters of MEG, force field parameters of the solute have to be considered as well. For $CO_2$, TraPPE force field parameters are obtained using pure component data and not data of multicomponent systems. Predictions of MC simulations can be improved by revising force field parameterization or considering different force field combinations. Alternatively, one might consider changes to the combination rules used. Here, the Lorentz−Berthelot rules are used to compute interactions between dissimilar sites. To improve the predictions of MC simulations, other combination rules can be considered and/or adjustable parameter(s) can be added to fine-tune solute−solvent interactions.

**4.2. Solubility of $CH_4$, $H_2S$, and $N_2$ in MEG from MC Simulations.** MC simulations were used to compute the solubility of other pure gases in MEG at 373.15 K. MC simulation results were compared to experimental data from the literature.

In Figure 6, the absorption isotherm of $CH_4$ in MEG is shown for $T = 373.15$ K and pressures ranging from 1 to 10
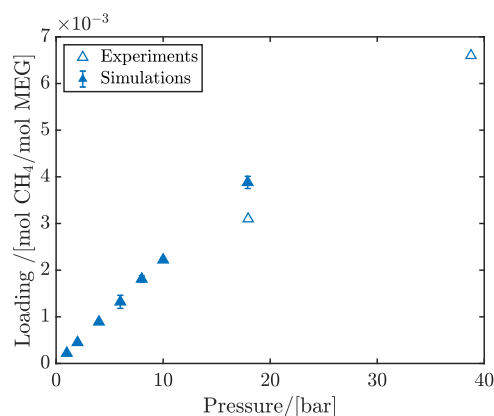


**Figure 6.** Absorption isotherm of $CH_4$ in MEG at $T = 373.15$ K. Closed symbols are solubilities from MC simulations in the osmotic ensemble (details in Section 3), and open symbols are experimental data from ref 68. The raw data and the corresponding uncertainties are provided in Tables S11 and S17 of the Supporting Information.

bar. At this pressure range, low loadings of $CH_4$ are obtained from MC simulations. To validate computational results, experimental solubilities[68] at higher pressures are shown in Figure 6. At $P = 17.9$ bar, MC simulations overpredict the solubility of $CH_4$ in MEG by 25%. As discussed earlier in Section 4.1, higher absorption of solutes is due to the underestimated densities of MEG when using the TraPPE-UA force field.

In Figure 7, solubilities of $H_2S$ in MEG at $T = 373.15$ K from MC simulations using two different $H_2S$ force fields are compared to experimental solubilities from ref 15. A reasonable agreement between MC simulations and experiments is obtained for the two force fields, but larger deviations increase at high pressures. The $H_2S$-TraPPE force field underpredicts loadings of $H_2S$, while the $H_2S$-KL force field overpredicts loadings under the studied conditions. At atmospheric pressure, solubilities computed using $H_2S$-KL were found to be closer to the experimental value reported by Jou et al.,[15] compared to the solubility computed using $H_2S$-TraPPE.

In Figure 8, the absorption isotherm of $N_2$ in MEG at $T = 373.15$ K is shown. The loading of $N_2$ is computed using MC simulations and is compared to experimental data from Zheng et al.[6] Because the absorption of $N_2$ in MEG is negligible at atmospheric pressures, simulations were performed at pressures ranging from 10 to 100 bar. From Figure 8, it can be seen that the computed loadings deviate considerably from experimental values and that the deviations increase systematically with pressure. As discussed earlier, differences between MC simulations and experimental data at high pressures can be improved by modifying the used force fields or fine-tuning solute−solvent interactions.
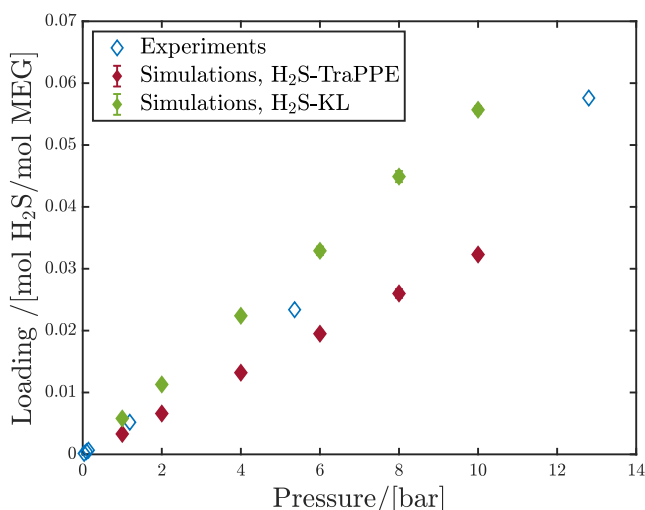
**Figure 7.** Absorption isotherm of $H_2S$ in MEG at $T$ = 373.15 K. Closed symbols are solubilities from MC simulations (details in Section 3) using two force fields: $H_2S$-TraPPE and $H_2S$-KL.[46] Open symbols are experimental data from ref 9. The raw data and the corresponding uncertainties are provided in Tables S13 and S18 of the Supporting Information.



**Figure 8.** Absorption isotherm of $N_2$ in MEG at $T$ = 373.15 K. Closed symbols are solubilities from MC simulations (details in Section 3), and open symbols are experimental data from ref 6. The raw data and the corresponding uncertainties are provided in Tables S12 and S19 of the Supporting Information.
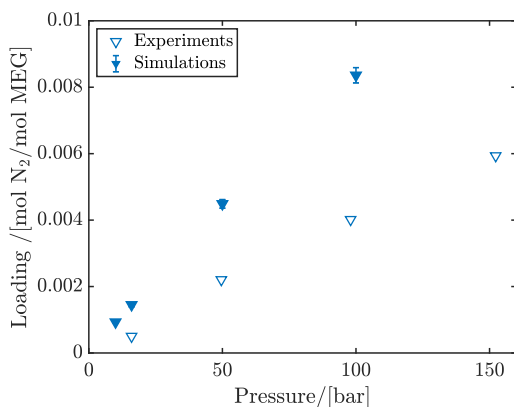
In Table 5, Henry coefficients computed using MC simulations of $CH_4$, $H_2S$, and $N_2$ are listed. Experimental Henry coefficients of $CH_4$ and $H_2S$ are also shown. The average differences between experimental and computational values are around 25%. From Henry coefficients at $T$ = 373.15 K, the following order of solubility is exhibited: $H_2S$ > $CO_2$ >

**Table 5. Henry Coefficients of Various Solutes in MEG Obtained from Experiments and MC Simulations**[a]

| | $H_{i,j}$, bar (mol $i$/mol EG) | |
|---|---|---|
| solute | experimental | MC simulations |
| $CH_4$ | 5673 | 4504 ± 165 |
| $H_2S$-TraPPE | 227.4 | 302 ± 14 |
| $H_2S$-KL | 227.4 | 173 ± 5 |
| $N_2$ | | 10,815 ± 248 |

[a]Experimental values are taken from refs 6 and[68] for $CH_4$ and $H_2S$, respectively.

$CH_4$ > $N_2$. From Henry coefficients, the ideal selectivity of the desired component $i$ in the undesired component $j$ can be expressed as

$$S_{i/j} = \left[ \frac{H_j}{H_i} \right]_T \tag{6}$$

In Table 6, ideal selectivities for the separation of $CO_2$ using MEG are provided, which are computed using Henry

**Table 6. Ideal Selectivities of $CO_2$, $CH_4$, $H_2S$, and $N_2$ in MEG Computed Using Henry Coefficients from Experiments and MC Simulations at $T$ = 373.15 K**[a]

| | $S_{i/j}$ | |
|---|---|---|
| separation | experimental | MC simulations |
| $CO_2$/$CH_4$ | 6.73 | 6.17 |
| $CO_2$/$H_2S$-TraPPE | 0.27 | 0.41 |
| $CO_2$/$H_2S$-KL | 0.27 | 0.24 |
| $CO_2$/$N_2$ | | 14.81 |

[a]Experimental values are taken from refs 6 and[68] for $CH_4$ and $H_2S$, respectively.

coefficients from experiments and MC simulations. The results show that $CO_2$ is more selectively absorbed in MEG than $CO_4$ and $N_2$. However, this is not true for the separation of $CO_2$ using MEG in the presence of $H_2S$.

## 5. CONCLUSIONS

In this work, the solubility of $CO_2$ in MEG was studied both experimentally and computationally. MC simulations in the osmotic ensemble were performed to predict the absorption of $CO_2$ as well as the absorption of $CH_4$, $H_2S$, and $N_2$. The CFCMC method was used to facilitate the insertion/deletion of particles into the solvent. TraPPE force fields were used to model all species. For $H_2S$, two force fields were compared: $H_2S$-TraPPE[69] and $H_2S$-KL.[46] The solubility of $CO_2$ in MEG was measured at the following temperatures: 333.15, 353.15, and 373.15 K. From experiments and MC simulations, $CO_2$ was found to be better absorbed at lower temperatures. At $T$ = 373.15 K, $CO_2$ and $H_2S$ were found to have higher solubilities in MEG than $CH_4$ and $N_2$. Solubilities predicted by MC simulations are in reasonable agreement with experimental data. For all the solutes studied in this work, deviations between MC simulations and experiments were found to increase with pressure. For the solubility of $H_2S$, predictions from the $H_2S$-KL force field were closer to experimental measurements than those from $H_2S$-TraPPE. Other than absorption isotherms, Henry coefficients were also computed. The order of solubilities of the gases in MEG at 373.15 K was found to be as follows: $H_2S$ > $CO_2$ > $CH_4$ > $N_2$. The average difference between Henry coefficients from experiments and Henry coefficients from MC simulations is around 20%. These results can be regarded satisfactory, considering that force fields from the literature were directly used without fitting binary interaction parameters. To improve predictions at high pressures, force field adjustments are required. For the solubility of $CO_2$ in MEG, the experimental data provided in this work may be used to generate new force field parameters.

## ASSOCIATED CONTENT

**Ⓢ Supporting Information**

The Supporting Information is available free of charge at https://pubs.acs.org/doi/10.1021/acs.jced.0c00771.

Derivation of an expression to estimate the saturated vapor pressure from CFCMC simulations, force field parameters, expanded uncertainty calculations, tabulated experimental data, and simulation results (PDF)

## AUTHOR INFORMATION

**Corresponding Author**

**Thijs J. H. Vlugt** − *Engineering Thermodynamics, Process & Energy Department, Faculty of Mechanical, Maritime and Materials Engineering, Delft University of Technology, 2628 CB Delft, The Netherlands;* ⓘ orcid.org/0000-0003-3059-8712; Email: t.j.h.vlugt@tudelft.nl

**Authors**

**Noura Dawass** − *Engineering Thermodynamics, Process & Energy Department, Faculty of Mechanical, Maritime and Materials Engineering, Delft University of Technology, 2628 CB Delft, The Netherlands*

**Ricardo R. Wanderley** − *Department of Chemical Engineering, Norwegian University of Science and Technology, 7034 Trondheim, Norway;* ⓘ orcid.org/0000-0002-8579-1715

**Mahinder Ramdin** − *Engineering Thermodynamics, Process & Energy Department, Faculty of Mechanical, Maritime and Materials Engineering, Delft University of Technology, 2628 CB Delft, The Netherlands;* ⓘ orcid.org/0000-0002-8476-7035

**Othonas A. Moultos** − *Engineering Thermodynamics, Process & Energy Department, Faculty of Mechanical, Maritime and Materials Engineering, Delft University of Technology, 2628 CB Delft, The Netherlands;* ⓘ orcid.org/0000-0001-7477-9684

**Hanna K. Knuutila** − *Department of Chemical Engineering, Norwegian University of Science and Technology, 7034 Trondheim, Norway;* ⓘ orcid.org/0000-0003-2057-1743

Complete contact information is available at:
https://pubs.acs.org/10.1021/acs.jced.0c00771

**Notes**

The authors declare no competing financial interest.

## REFERENCES

(1) Ethylene Glycol. https://www.chemicalsafetyfacts.org/ethylene-glycol/ Visited on 11/08, 2020.

(2) Monoethylene Glycol (MEG) Market by Major Drivers 2020—Global Industry Insights by Global Players, Regional Segmentation, Growth, Applications, Value and Forecasts till 2026. https://www-marketwatch-com.tudelft.idm.oclc.org/press-release/monoethylene-glycol-meg-market-by-major-drivers-2020—global-industry-insights-by-global-players-regional-segmentation-growth-applications-value-and-forecasts-till-2026-2020-08-03 (accessed 11/08, 2020).

(3) Yue, H.; Zhao, Y.; Ma, X.; Gong, J. Ethylene glycol: properties, synthesis, and applications. *Chem. Soc. Rev.* **2012**, *41*, 4218−4244.

(4) Cha, M.; Shin, K.; Kim, J.; Chang, D.; Seo, Y.; Lee, H.; Kang, S.-P. Thermodynamic and kinetic hydrate inhibition performance of aqueous ethylene glycol solutions for natural gas. *Chem. Eng. Sci.* **2013**, *99*, 184−190.

(5) Afzal, W.; Breil, M. P.; Théveneau, P.; Mohammadi, A. H.; Kontogeorgis, G. M.; Richon, D. Phase equilibria of mixtures containing glycol and n−alkane: experimental study of infinite dilution activity coefficients and modeling using the cubic−plus−association equation of state. *Ind. Eng. Chem. Res.* **2009**, *48*, 11202−11210.

(6) Zheng, D.-Q.; Ma, W.-D.; Wei, R.; Guo, T.-M. Solubility study of methane, carbon dioxide and nitrogen in ethylene glycol at elevated temperatures and pressures. *Fluid Phase Equilib.* **1999**, *155*, 277−286.

(7) Afzal, W.; Breil, M. P.; Tsivintzelis, I.; Mohammadi, A. H.; Kontogeorgis, G. M.; Richon, D. Experimental study and phase equilibrium modeling of systems containing acid gas and glycol. *Fluid Phase Equilib.* **2012**, *318*, 40−50.

(8) Henni, A.; Tontiwachwuthikul, P.; Chakma, A. Solubilities of carbon dioxide in polyethylene glycol ethers. *Can. J. Chem. Eng.* **2005**, *83*, 358−361.

(9) Xu, H.-J.; Zhang, C.-F.; Zheng, Z.-S. Solubility of hydrogen sulfide and carbon dioxide in a solution of methyldiethanolamine mixed with ethylene glycol. *Ind. Eng. Chem. Res.* **2002**, *41*, 6175−6180.

(10) Lin, C.-M.; Leron, R. B.; Caparanga, A. R.; Li, M.-H. Henry's constant of carbon dioxide-aqueous deep eutectic solvent (choline chloride/ethylene glycol, choline chloride/glycerol, choline chloride/malonic acid) systems. *J. Chem. Thermodyn.* **2014**, *68*, 216−220.

(11) Leron, R. B.; Li, M.-H. Solubility of carbon dioxide in a choline chloride−ethylene glycol based deep eutectic solvent. *Thermochim. Acta* **2013**, *551*, 14−19.

(12) Nagumo, R.; Muraki, Y.; Iwata, S.; Mori, H.; Takaba, H.; Yamada, H. Molecular Dynamics Simulation Study on $CO_2$ Physical Absorption Mechanisms for Ethylene-Glycol−Based Solvents Using Free Energy Calculations. *Ind. Eng. Chem. Res.* **2016**, *55*, 8200−8206.

(13) Skylogianni, E.; Wanderley, R. R.; Austad, S. S.; Knuutila, H. K. Density and Viscosity of the Nonaqueous and Aqueous Mixtures of Methyldiethanolamine and Monoethylene Glycol at Temperatures from 283.15 to 353.15 K. *J. Chem. Eng. Data* **2019**, *64*, 5415−5431.

(14) Skylogianni, E.; Perinu, C.; Cervantes Gameros, B. Y.; Knuutila, H. K. Carbon Dioxide solubility in mixtures of methyldiethanolamine with monoethylene glycol, monoethylene glycol−water and triethylene glycol. *J. Chem. Thermodyn.* **2020**, *151*, 106176.

(15) Jou, F.-Y.; Deshmukh, R. D.; Otto, F. D.; Mather, A. E. Vapor−Liquid Equilibria of $H_2S$ and $CO_2$ and Ethylene Glycol At Elevated Pressures. *Chem. Eng. Commun.* **1990**, *87*, 223−231.

(16) Reid, R. C.; Prausnitz, J. M.; Poling, B. E. *The Properties of Gases and Liquids*; McGraw Hill Book Co., 1987.

(17) Ungerer, P.; Nieto-Draghi, C.; Rousseau, B.; Ahunbay, G.; Lachet, V. Molecular simulation of the thermophysical properties of fluids: From understanding toward quantitative predictions. *J. Mol. Liq.* **2007**, *134*, 71−89.

(18) Yarveicy, H.; Ghiasi, M. M.; Mohammadi, A. H. Performance evaluation of the machine learning approaches in modeling of $CO_2$ equilibrium absorption in Piperazine aqueous solution. *J. Mol. Liq.* **2018**, *255*, 375−383.

(19) Yarveicy, H.; Saghafi, H.; Ghiasi, M. M.; Mohammadi, A. H. Decision tree−based modeling of $CO_2$ equilibrium absorption in different aqueous solutions of absorbents. *Environ. Prog. Sustainable Energy* **2019**, *38*, S441−S448.

(20) Allen, M. P.; Tildesley, D. J. *Computer Simulation of Liquids*, 2nd ed.; Oxford University Press: New York, USA, 2017.

(21) Frenkel, D.; Smit, B. *Understanding Molecular Simulation: from Algorithms to Applications*, 2nd ed.; Academic Press: London, U.K., 2002; Vol. *1*.

(22) Shi, W.; Maginn, E. J. Molecular simulation and regular solution theory modeling of pure and mixed gas absorption in the

ionic liquid 1−n−hexyl−3−methylimidazolium bis (trifluoromethyl-sulfonyl) amide ([hmim] [Tf₂N]). *J. Phys. Chem. B* **2008**, *112*, 16710−16720.

(23) Maginn, E. J. Molecular simulation of ionic liquids: current status and future opportunities. *J. Phys.: Condens. Matter* **2009**, *21*, 373101.

(24) Shi, W.; Maginn, E. J. Continuous Fractional Component Monte Carlo: an adaptive biasing method for open system atomistic simulations. *J. Chem. Theory Comput.* **2007**, *3*, 1451−1463.

(25) Ramdin, M.; Balaji, S. P.; Torres-Knoop, A.; Dubbeldam, D.; de Loos, T. W.; Vlugt, T. J. H. Solubility of natural gas species in ionic liquids and commercial solvents: experiments and Monte Carlo simulations. *J. Chem. Eng. Data* **2015**, *60*, 3039−3045.

(26) Zhang, L.; Siepmann, J. I. Direct calculation of Henry's law constants from Gibbs ensemble Monte Carlo simulations: nitrogen, oxygen, carbon dioxide and methane in ethanol. *Theor. Chem. Acc.* **2006**, *115*, 391−397.

(27) Jamali, S. H.; Ramdin, M.; Becker, T. M.; Torres-Knoop, A.; Dubbeldam, D.; Buijs, W.; Vlugt, T. J. H. Solubility of sulfur compounds in commercial physical solvents and an ionic liquid from Monte Carlo simulations. *Fluid Phase Equilib.* **2017**, *433*, 50−55.

(28) Shah, M. S.; Tsapatsis, M.; Siepmann, J. I. Monte Carlo simulations probing the adsorptive separation of hydrogen sulfide/methane mixtures using all−silica zeolites. *Langmuir* **2015**, *31*, 12268−12278.

(29) Kapoor, U.; Shah, J. K. Monte Carlo Simulations of Pure and Mixed Gas Solubilities of $CO_2$ and $CH_4$ in Nonideal Ionic Liquid−Ionic Liquid Mixtures. *Ind. Eng. Chem. Res.* **2019**, *58*, 22569−22578.

(30) Salehi, H. S.; Hens, R.; Moultos, O. A.; Vlugt, T. J. H. Computation of gas solubilities in choline chloride urea and choline chloride ethylene glycol Deep Eutectic Solvents using Monte Carlo simulations. *J. Mol. Liq.* **2020**, *316*, 113729.

(31) Dubbeldam, D.; Torres-Knoop, A.; Walton, K. S. On the inner workings of Monte Carlo codes. *Mol. Simul.* **2013**, *39*, 1253−1292.

(32) Poursaeidesfahani, A.; Torres-Knoop, A.; Dubbeldam, D.; Vlugt, T. J. H. Direct free energy calculation in the Continuous Fractional Component Gibbs ensemble. *J. Chem. Theory Comput.* **2016**, *12*, 1481−1490.

(33) Shi, W.; Maginn, E. J. Improvement in molecule exchange efficiency in Gibbs Ensemble Monte Carlo: development and implementation of the continuous fractional component move. *J. Comput. Chem.* **2008**, *29*, 2520−2530.

(34) Hens, R.; Rahbari, A.; Caro-Ortiz, S.; Dawass, N.; Erdős, M.; Poursaeidesfahani, A.; Salehi, H. S.; Celebi, A. T.; Ramdin, M.; Moultos, O. A.; Dubbeldam, D.; Vlugt, T. J. H. Brick−CFCMC: Open source software for Monte Carlo simulations of phase and reaction equilibria using the Continuous Fractional Component method. *J. Chem. Inf. Model.* **2020**, *60*, 2678−2682.

(35) Rahbari, A.; Hens, R.; Nikolaidis, I. K.; Poursaeidesfahani, A.; Ramdin, M.; Economou, I. G.; Moultos, O. A.; Dubbeldam, D.; Vlugt, T. J. H. Computation of partial molar properties using Continuous Fractional Component Monte Carlo. *Mol. Phys.* **2018**, *116*, 3331−3344.

(36) Rahbari, A.; Hens, R.; Ramdin, M.; Moultos, O. A.; Dubbeldam, D.; Vlugt, T. J. H. Recent advances in the Continuous Fractional Component Monte Carlo methodology. *Mol. Simul.* **2020**, 1. , in press

(37) Martin, M. G.; Siepmann, J. I. Transferable potentials for phase equilibria. 1. United−atom description of n−alkanes. *J. Phys. Chem. B* **1998**, *102*, 2569−2577.

(38) Stubbs, J. M.; Potoff, J. J.; Siepmann, J. I. Transferable potentials for phase equilibria. 6. United−atom description for ethers, glycols, ketones, and aldehydes. *J. Phys. Chem. B* **2004**, *108*, 17596−17605.

(39) Yang, Q.; Zhong, C. Molecular simulation of carbon dioxide/methane/hydrogen mixture adsorption in metal−organic frameworks. *J. Phys. Chem. B* **2006**, *110*, 17776−17783.

(40) Kamath, G.; Ketko, M.; Baker, G. A.; Potoff, J. J. Monte Carlo predictions of phase equilibria and structure for dimethyl ether+

sulfur dioxide and dimethyl ether+ carbon dioxide. *J. Chem. Phys.* **2012**, *136*, 044514.

(41) Michalis, V. K.; Tsimpanogiannis, I. N.; Stubos, A. K.; Economou, I. G. Direct phase coexistence molecular dynamics study of the phase equilibria of the ternary methane−carbon dioxide−water hydrate system. *Phys. Chem. Chem. Phys.* **2016**, *18*, 23538−23548.

(42) Wang, S.; Lu, L.; Wu, D.; Lu, X.; Cao, W.; Yang, T.; Zhu, Y. Molecular simulation study of the adsorption and diffusion of a mixture of $CO_2/CH_4$ in activated carbon: effect of textural properties and surface chemistry. *J. Chem. Eng. Data* **2016**, *61*, 4139−4147.

(43) Moultos, O. A.; Tsimpanogiannis, I. N.; Panagiotopoulos, A. Z.; Economou, I. G. Atomistic molecular dynamics simulations of $CO_2$ diffusivity in $H_2O$ for a wide range of temperatures and pressures. *J. Phys. Chem. B* **2014**, *118*, 5532−5541.

(44) Nikolaidis, I. K.; Poursaeidesfahani, A.; Csaszar, Z.; Ramdin, M.; Vlugt, T. J. H.; Economou, I. G.; Moultos, O. A. Modeling the phase equilibria of asymmetric hydrocarbon mixtures using molecular simulation and equations of state. *AIChE J.* **2019**, *65*, 792−803.

(45) Cardona, J.; Fartaria, R.; Sweatman, M. B.; Lue, L. Molecular dynamics simulations for the prediction of the dielectric spectra of alcohols, glycols and monoethanolamine. *Mol. Simul.* **2016**, *42*, 370−390.

(46) Kristóf, T.; Liszi, J. Effective intermolecular potential for fluid hydrogen sulfide. *J. Phys. Chem. B* **1997**, *101*, 5480−5483.

(47) Vorholz, J.; Rumpf, B.; Maurer, G. Prediction of the vapor−liquid phase equilibrium of hydrogen sulfide and the binary system water−hydrogen sulfide by molecular simulation. *Phys. Chem. Chem. Phys.* **2002**, *4*, 4449−4457.

(48) Faure, F.; Rousseau, B.; Lachet, V.; Ungerer, P. Molecular Simulation of the solubility and diffusion of carbon dioxide and hydrogen sulfide in polyethylene melts. *Fluid Phase Equilib.* **2007**, *261*, 168−175.

(49) Kim, I.; Svendsen, H. F. Heat of absorption of carbon dioxide ($CO_2$) in monoethanolamine (MEA) and 2−(aminoethyl) ethanolamine (AEEA) solutions. *Ind. Eng. Chem. Res.* **2007**, *46*, 5803−5809.

(50) Kim, I.; Hoff, K. A.; Mejdell, T. Heat of absorption of $CO_2$ with aqueous solutions of MEA: new experimental data. *Energy Procedia* **2014**, *63*, 1446−1455.

(51) Wick, C. D.; Martin, M. G.; Siepmann, J. I. Transferable potentials for phase equilibria. 4. United−atom description of linear and branched alkenes and alkylbenzenes. *J. Phys. Chem. B* **2000**, *104*, 8008−8016.

(52) Gross, J.; Sadowski, G. Perturbed-chain SAFT: An equation of state based on a perturbation theory for chain molecules. *Ind. Eng. Chem. Res.* **2001**, *40*, 1244−1260.

(53) Diamantonis, N. I.; Boulougouris, G. C.; Mansoor, E.; Tsangaris, D. M.; Economou, I. G. Evaluation of cubic, SAFT, and PC-SAFT equations of state for the vapor−liquid equilibrium modeling of $CO_2$ mixtures with other gases. *Ind. Eng. Chem. Res.* **2013**, *52*, 3933−3942.

(54) Shi, W.; Maginn, E. J. Atomistic Simulation of the Absorption of Carbon Dioxide and Water in the Ionic Liquid 1-n-Hexyl-3-methylimidazolium Bis (trifluoromethylsulfonyl) imide ([hmim] [Tf2N]. *J. Phys. Chem. B* **2008**, *112*, 2045−2055.

(55) Torres-Knoop, A.; Balaji, S. P.; Vlugt, T. J. H.; Dubbeldam, D. A comparison of advanced Monte Carlo methods for open systems: CFCMC vs CBMC. *J. Chem. Theory Comput.* **2014**, *10*, 942−952.

(56) Pham, T. T.; Shirts, M. R. Identifying low variance pathways for free energy calculations of molecular transformations in solution phase. *J. Chem. Phys.* **2011**, *135*, 034114.

(57) Rahbari, A.; Hens, R.; Jamali, S. H.; Ramdin, M.; Dubbeldam, D.; Vlugt, T. J. H. Effect of truncating electrostatic interactions on predicting thermodynamic properties of water−methanol systems. *Mol. Simul.* **2019**, *45*, 336−350.

(58) Shirts, M. R.; Pitera, J. W.; Swope, W. C.; Pande, V. S. Extremely precise free energy calculations of amino acid side chain analogs: Comparison of common molecular mechanics force fields for proteins. *J. Chem. Phys.* **2003**, *119*, 5740−5761.

(59) Shirts, M. R.; Pande, V. S. Solvation free energies of amino acid side chain analogs for common molecular mechanics water models. *J. Chem. Phys.* **2005**, *122*, 134508.

(60) Lias, S. G.; Bartmess, J. E.; Liebman, J. F.; Holmes, J. L.; Levin, R. D.; Mallard, W. G. *NIST Chemistry WebBook, NIST Standard Reference Database Number 69*; National Institute of Standards and Technology: Gaithersburg MD, 2018; p 20899.

(61) Wanderley, R. R.; Pinto, D. D. D.; Knuutila, H. K. Investigating opportunities for water-lean solvents in $CO_2$ capture: VLE and heat of absorption in water-lean solvents containing MEA. *Sep. Purif. Technol.* **2020**, *231*, 115883.

(62) Wise, M.; Chapoy, A. Phase Behavior of $CO_2$ in Monoethylene Glycol between 263.15−343.15 K and 0.2−40.3 MPa: An Experimental and Modeling Approach. *J. Chem. Eng. Data* **2017**, *62*, 4154−4159.

(63) Serpa, F. S.; Vidal, R. S.; Filho, J. H. B. A.; Nascimento, J. F. d.; Ciambelli, J. R. P.; Figueiredo, C. M. S.; Salazar-Banda, G. R.; Santos, A. F.; Fortuny, M.; Franceschi, E.; et al. Solubility of carbon dioxide in ethane-1, 2-diol−water mixtures. *J. Chem. Eng. Data* **2013**, *58*, 3464−3469.

(64) Prausnitz, J. M.; Lichtenthaler, R. N.; De Azevedo, E. G. *Molecular Thermodynamics of fluid−phase Equilibria*, 3rd ed.; Pearson Education: Upper Saddle River, N.J, 1998.

(65) Shing, K. S.; Gubbins, K. E.; Lucas, K. Henry constants in non-ideal fluid mixtures. *Mol. Phys.* **1988**, *65*, 1235−1252.

(66) Ramdin, M.; Balaji, S. P.; Vicent-Luna, J. M.; Gutiérrez-Sevillano, J. J.; Calero, S.; de Loos, T. W.; Vlugt, T. J. H. Solubility of the precombustion gases $CO_2$, $CH_4$, CO, $H_2$, $N_2$, and $H_2S$ in the ionic liquid [bmim] [$Tf_2$N] from Monte Carlo simulations. *J. Phys. Chem. C* **2014**, *118*, 23599−23604.

(67) Wanderley, R. R.; Evjen, S.; Pinto, D. D. D.; Knuutila, H. K. The Salting−out Effect in Some Physical Absorbents for $CO_2$ Capture. *Chem. Eng. Trans.* **2018**, *69*, 97−102.

(68) Galvão, A. C.; Francesconi, A. Z. Solubility of methane and carbon dioxide in ethylene glycol at pressures up to 14 MPa and temperatures ranging from (303 to 423) K. *J. Chem. Thermodyn.* **2010**, *42*, 684−688.

(69) Shah, M. S.; Tsapatsis, M.; Siepmann, J. I. Development of the Transferable Potentials for Phase Equilibria Model for Hydrogen Sulfide. *J. Phys. Chem. B* **2015**, *119*, 7041−7052.

(70) Potoff, J. J.; Siepmann, J. I. Vapor−liquid equilibria of mixtures containing alkanes, carbon dioxide, and nitrogen. *AIChE J.* **2001**, *47*, 1676−1682.

(71) Dubbeldam, D.; Calero, S.; Vlugt, T. J. H. iRASPA: GPU−accelerated visualization software for materials scientists. *Mol. Simul.* **2018**, *44*, 653−676.